*Kovove Mater. 58 2020 331–339*
*DOI: 10.4149/km_2020_5_331*



# Characterization of complex $Al_{60}Cu_{20}Ni_{15}Ti_5$ alloy produced by mechanical alloying and sintering

M. Okumuş[1]*, F. Demir[1], M. Göğebakan[2]

[1]*Department of Metallurgical and Materials Engineering, Batman University, Batman, Turkey*
[2]*Department of Physics, Kahramanmaraş Sutcu Imam University, Kahramanmaraş, Turkey*

Received 27 March 2020, received in revised form 13 June 2020, accepted 17 June 2020

**Abstract**

In this work, microstructural and thermal properties of the mechanically alloyed complex $Al_{60}Cu_{20}Ni_{15}Ti_5$ alloy have been investigated by a combination of differential thermal analysis (DTA), X-ray diffraction (XRD), and scanning electron microscope with energy dispersive X-ray detection (SEM/EDX). The results showed that the new $Al_{60}Cu_{20}Ni_{15}Ti_5$ alloy in metastable multiphase formation was produced by milling for 50 h. As the milling time increased from 50 h to 100 h, more homogeneous structure and intermetallic phases such as $Al_3Ni$ and $Al_2Cu$ were observed, and also grain size decreased. Besides, the maximum microhardness value in pressed and sintered alloy samples was found to be 560 HV.

K e y w o r d s: Al-based alloys, thermal properties, microstructure, mechanical alloying

## 1. Introduction

In a large number of commercial alloys, Al-based alloys have attracted considerable attention due to their significant mechanical behavior, significant chemical properties, and useful physical properties, which can lead to application in some different fields [1–4]. Al-alloys have a high strength/weight ratio, which is an important parameter for material selection and design [5]. In addition to some superior properties of Al-alloys, titanium (Ti) also has good corrosion resistance, low density, and high strength/weight ratio. It, therefore, is used in many applications such as automotive, aerospace, and submarine [6–8]. It is well known that the behavior of Al-alloys, such as maximum tensile stress and corrosion resistance, is limited.

For this reason, it is possible to produce superior complex Al-based alloy materials. In recent years, new studies have been performed to deliver higher performance materials such as Al-alloy-based metal matrix composites or nanocrystal dispersed amorphous alloys [9–11]. Al-alloy-based composites to satisfy the increasing demand for developing technology continue to attract researchers, although there are many parallel research areas. The other materials, like amorphous or nanocrystalline intermetallics [12, 13], chose for themselves different areas of application. It is very important to better understand the precipitation phenomena in multiphase alloys [14] and make them applicable in engineering. Therefore, complex Al-based alloys remain the most potential candidates to be investigated. From this point of view, this study aims to produce and characterize the complex Al-Cu-Ni-Ti alloy.

Al-based alloys can be produced by different techniques such as mechanical alloying [15, 16], arc melting [17], melt spinning [18], laser cladding [19], fluxed water quenching [20]. In mechanical alloying (MA), materials are prepared in powder forms, which can be easily pressed in desired dimensions and shapes for practical applications [21]. Therefore, many studies have been made on designing nanocrystalline, quasicrystalline, and amorphous materials by using the MA method. Al-Cu-based alloys such as Al-Cu-Ti [22], Al-Cu-Fe [23, 24] have been studied in detail; however, a few works have been done on intermetallic phase formation in Al-Cu-based alloys. Among metallic materials, Ti and its alloys are shown to be the most suitable candidates for the production of less weighted composition for automotive and aerospace

*Corresponding author: e-mail address: mustafa.okumus@batman.edu.tr

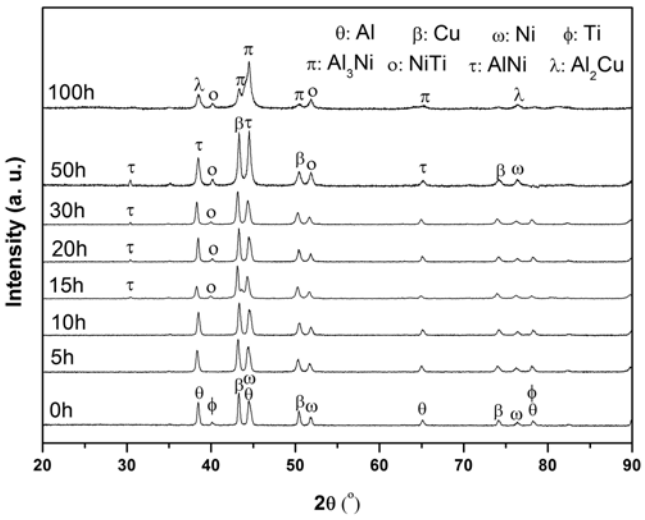


Fig. 1. XRD patterns of mechanically milled $Al_{60}Cu_{20}Ni_{15}Ti_5$ powders as a function of milling time.

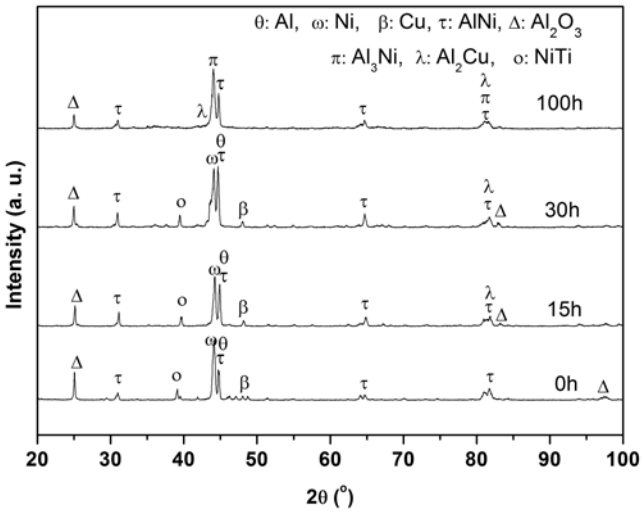


Fig. 2. XRD patterns of sintered $Al_{60}Cu_{20}Ni_{15}Ti_5$ powders as a function of milling time.

applications. By adding Ti material to NiAl alloys, the creep resistance properties of these alloys are increased as well as other properties [25]. Hence, the mechanically milled Al-Cu-Ni-Ti powder, which has never been studied, is a better choice for technological applications as materials with excellent wear resistance, high strength, high hardness, high thermal stability, low density, and good electromagnetic properties. According to the reported literature [26–30], the high entropy alloys have provided these properties.

Furthermore, it has been reported that $Al_{65}Cu_{20}Ti_{15}$ alloy [31] prepared by the MA technique exhibits a relatively high compressive strength of 1745 MPa among Al-based alloys, and the $Al_{65}Cu_{20}Ti_{15}$ composite [32] consisting of intermetallic phases is also stable after 50 hours of ball milling. The complex Al--Cu-Ni-Ti alloys can also provide some of the properties mentioned above. So, in this study, the complex $Al_{60}Cu_{20}Ni_{15}Ti_5$ alloys were fabricated by the MA method and characterized.

## 2. Experimental

Al-Cu-Ni-Ti elemental powders in the nominal stoichiometry of $Al_{60}Cu_{20}Ni_{15}Ti_5$ (at.%) were weighed and subjected to mechanical alloying under argon (Ar) atmosphere to avoid oxidation in an XQM-2 high--energy planetary ball mill operated at 350 rpm with 10 : 1 ball to powder weight ratio. Then, the mechanically alloyed powders were put into a steel cylinder can and were pressed under 250 MPa in a high-pressure device to consolidate the powders. The pressed powders were sintered at a temperature of 700 ℃ for 1 h in the air atmosphere in a high-temperature furnace and afterward were polished. Surface analyses of polished samples were examined by using a Leica 180 DM LP polarized light microscopy. Microhardness measurements were conducted on a Shimadzu HMV-2 Vickers Hardness Tester under a load of 500 gf ($\sim$ 4.903 N). The obtained hardness value for each sintered alloy is an average of 10 measurements from different regions. Thermal properties of alloyed powders were analyzed by using an SII 6300 EXSTAR differential thermal analyzer (DTA), where the sample was heated at 30 ℃ min$^{-1}$ in a pure nitrogen atmosphere. Microstructural analyses were performed by using a Zeiss EVO LS10 scanning electron microscope equipped with an energy-dispersive X-ray spectrometer (SEM-EDX). The phase analyses were performed by an X-ray diffractometer, XRD (Philips X'Pert Pro diffractometer with $CuK_\alpha$ radiation).

## 3. Results and discussion

The formation of intermetallic phases in a complex alloy produced by the mechanical alloying method is strongly dependent on the processing parameters such as milling time and sintering temperature. In the present study, we have changed the milling time while keeping other parameters nominally constant. Figure 1 shows XRD results of the alloyed $Al_{60}Cu_{20}Ni_{15}Ti_5$ complexes produced using a high-energy planetary ball mill at different milling times in the range 0–100 h. The diffraction peaks which belong to pure crystalline, Al, Cu, Ni, and Ti elements are shown in the milling powders (0–10 h). As the milling time increases to 15 h, NiTi and AlNi intermetallic phases are observed simultaneously with the disappearance of pure Ti reflection peaks. This indicated

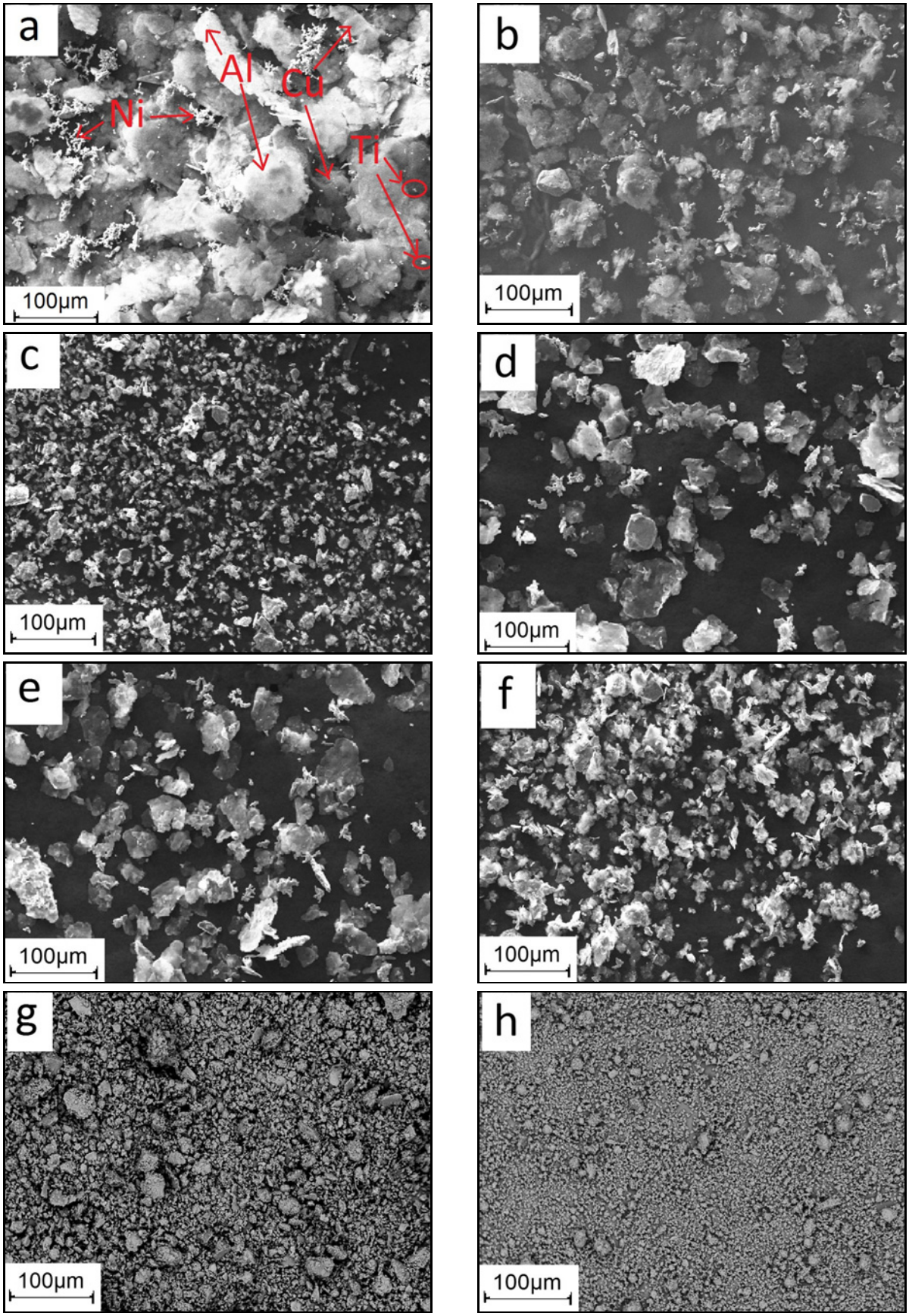


Fig. 3. SEM images of mechanically milled $Al_{60}Cu_{20}Ni_{15}Ti_5$ powders as a function of milling time: (a) 0 h, (b) 5 h, (c) 10 h, (d) 15 h, (e) 20 h, (f) 30 h, (g) 50 h, and (h) 100 h.

that in the first stage of milling, Ni reacted with Al and Ti to form the NiTi and AlNi intermetallic phases. However, the disappearance of the Ti reflection peaks occurs due to its small weight fraction in the powders mixture compared to other and also caused by significant particle and crystal refinement together with high lattice strain [33, 34].

In Fig. 1 on the XRD pattern after 50 h compared with XRD patterns from 15 to 30 h, there is a noticeable increase in the intensity of Cu and Ni peaks, in addition to the rise in the intensity of intermetallic AlNi and NiTi peaks. The reason for the increase in Cu and Ni peak intensities is the increase of the ratio of Cu and Ni in the powders mixture by the formation of AlNi- and NiTi-phases. When the milling time was increased to 100 h, the AlNi-phase was not observed. However, new phases indicating $Al_3Ni$ and $Al_2Cu$ intermetallic phases in the produced intermetallic complex alloys were observed. These results are in good agreement with reported similar studies [34, 35].

To investigate the structural change that occurs during heat treatment of alloyed $Al_{60}Cu_{20}Ni_{15}Ti_5$ alloys, the samples were annealed for 1 h at 700 ℃ and then examined by XRD. The XRD graphs for the samples are given in Fig. 2. As seen in Fig. 2, as a result of the pressing of the powder particles and welding of the short-distance particles by heat treatment, the intermetallic phases such as AlNi and NiTi have been observed in the most of sintered samples. When Fig. 2 is compared to Fig. 1, it can be seen that the NiTi--phase is observed in non-sintered samples milled for 15–100 h, but not in sintered sample milled for 100 h. Besides, the AlNi-phase was observed in the sintered samples while it was not observed in the sample, which was milled for 100 h and not sintered. However, it was determined that the peak numbers indicating the concentration of $Al_2Cu$-phase increased. The MA process applied to the powders before sintering was effective in reducing the concentrations of phases such as Al, Ni, Ti, Cu, and formation of NiTi- and AlNi-phases. While the Ti-phase was not observed in the sintered samples, the NiTi-phase was formed in all except the 100 h milled sample. In addition, the AlNi-, $Al_2Cu$-, and $Al_3Ni$-phases were formed by decreasing the Al- and Cu-phase concentration in the samples. Moreover, as can be seen in Fig. 2, the $Al_2O_3$-phase, which was not observed in the non-sintered samples, formed in all sintered samples due to the oxidation during sintering. These results are consistent with the similar studies reported in the literature [36–38].

The alloyed powders were subjected to morphological examination with scanning electron microscopy (SEM) to determine homogeneity, particle size, and microstructural evolutions after MA. Various SEM images of the alloyed powders are presented in Fig. 3. As seen in Fig. 3a, the shapes of non-ground powders are different, and they can be precisely identified by

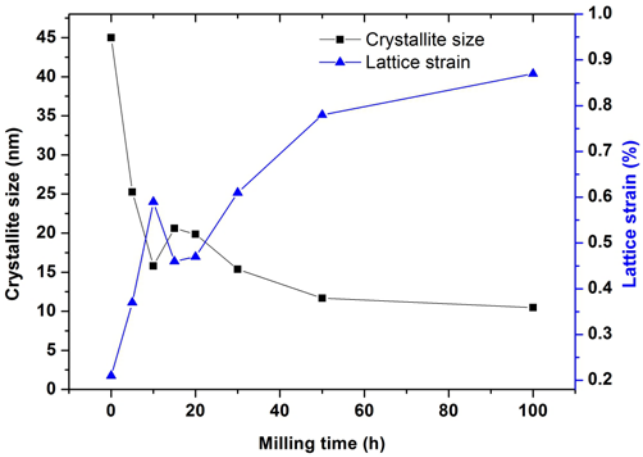


Fig. 4. The crystallite size and lattice strain of the mechanically milled $Al_{60}Cu_{20}Ni_{15}Ti_5$ powders as a function of milling time.

individual particles of Al, Cu, Ni, and Ti. After 5 h of milling, as the particles were fractured and welded, the structure of the powder had changed. At the stage of 10 h, the powders were more homogeneous, and the particle size decreased. At this stage, the collision force between all elemental powders and balls was mostly used in the deformation process. After 15 h of milling, Ni powder fused with the Al and Ti metals to form the AlNi- and NiTi-phases, and there was, therefore, an increase in aggregations and particle size. As seen in Fig. 3g, the microstructure of the $Al_{60}Cu_{20}Ni_{15}Ti_5$ alloy powder has become more homogeneous, and particle size decreases again. When the milling time is 100 h, the homogeneity increases, and the particles reach a more spherical structure. Also, larger-sized particles formed as a result of agglomerations are found in the structure. This reveals Cu, Ni, and Ti powders dissolve into the Al. Similar observations are reported for Mg-Cu-Ni powders [34]. These results are also in good agreement with the obtained XRD patterns of $Al_{60}Cu_{20}Ni_{15}Ti_5$ powder, as seen in Fig. 1.

The average lattice strain ($\varepsilon$) and crystallite size ($D$) evolution during ball milling of $Al_{60}Cu_{20}Ni_{15}Ti_5$ alloy powder is calculated from the broadening of XRD peaks using well-known equations [33, 39]. These equations are given as follows:

$$D = \frac{0.9\lambda}{\beta \cos\theta}, \tag{1}$$

$$\varepsilon = \frac{\beta}{4 \tan\theta}, \tag{2}$$

where $\lambda$ is the $CuK_\alpha$ radiation wavelength (0.154 nm), $\beta$ is the full width at half maximum intensity (FWHM), and $\theta$ is the Bragg diffraction angle. Generally, the XRD peak broadening is due to the instrumental broadening, broadening due to the lattice

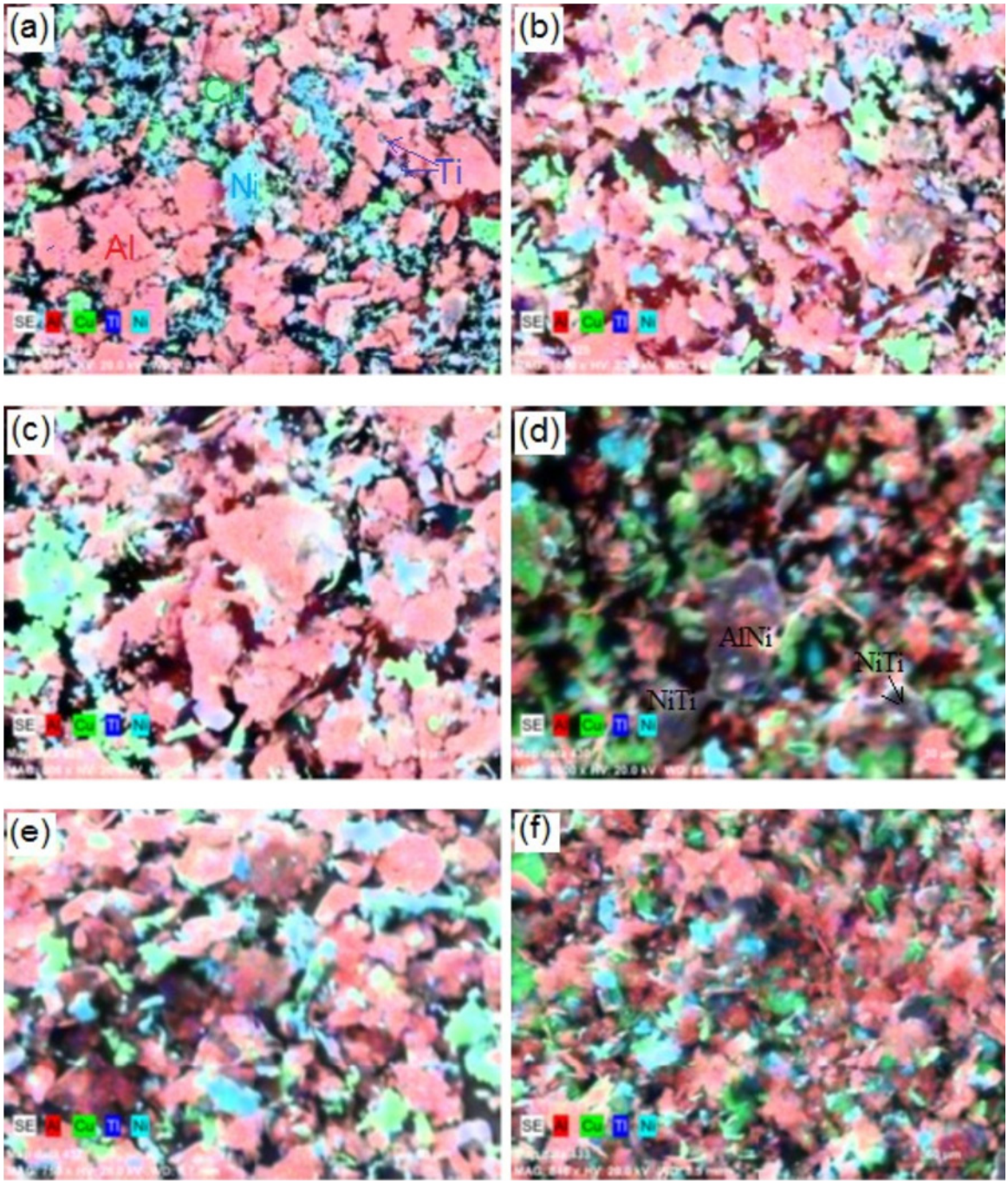


Fig. 5. EDX images of mechanically milled $Al_{60}Cu_{20}Ni_{15}Ti_5$ powders as a function of milling time: (a) 0 h, (b) 5 h, (c) 10 h, (d) 15 h, (e) 20 h, and (f) 30 h.

strain and the crystallite size present in the materials. The contributions of each of these effects are convoluted, causing an overall broadening of the XRD peaks. Therefore, estimating the crystallite size and the lattice strain, it is necessary to correct the instrumental effect. To estimate the instrumental corrected broadening $\beta$, one can see the equations [40–42] used in the separation methodology of the lattice strain ($\varepsilon$) and crystallite size ($D$) components in the broadening of XRD peaks.

Figure 4 exhibits the changing of crystallite size and lattice strain of the alloyed $Al_{60}Cu_{20}Ni_{15}Ti_5$ powders as a function of milling time. As shown in Fig. 4, while the crystallite size of alloyed powder decreases sharply and reaches 15.8 nm after 10 h milling, the lattice strain increases sharply and reaches 0.59 %. The sharp increase in the lattice strain and the decrease in the crystallite size of the powders indicate that as the milling time increases, severe plastic deformation and dislocations occur in the powder particles. However,

for 15–20 h of grinding, the crystallite size increases again rapidly, and the lattice strain decreases. This result indicates that the powders are recovered by heat treatment induced by high temperatures, there is a dynamic recovery by the rearrangement of dislocations [43], and new intermetallic phases are formed as a result of fusion. For 30 h, the crystallite size decreases to about 15.4 nm. With further milling time, it remains roughly constant because the refined powders tend to become balanceable. The crystallite size reaches the lowest value with 10.5 nm after 100 h of milling time. The lattice strain also reaches the maximum value with 0.87 %. As a result, since the $Al_{60}Cu_{20}Ni_{15}Ti_5$ powders were subjected to heavy mechanical deformation from the high-energy collisions during the MA process, the crystallite sizes decrease and the lattice strains increase as the milling time increased, which are in good agreement with reported similar results [8, 43]. Also, these results are inconsistent with present SEM observations.

To show the distribution of elemental powders in the complex alloy produced by MA, the EDX experiments were done. The EDX maps of the alloyed $Al_{60}Cu_{20}Ni_{15}Ti_5$ powders are presented in Fig. 5. As seen in Fig. 5a, the elemental powders Al, Cu, Ni, and Ti are randomly distributed before milling, and they are seen red, green, blue, and cyan colors, respectively. Figures 5b,c show that Al powder is still not homogeneous, but that Cu and Ti powders are homogeneous between each other and that Ni powders clustered in some regions. Although the color darkening shown in Fig. 5d cannot be defined by EDX, it is thought to indicate AlNi and NiTi intermetallic phases by considering the XRD and SEM results. Moreover, it is clear that the particle size increases due to the AlNi- and NiTi-phases. Figures 5e,f show that the particle size decreases again, and a more homogeneous structure is formed. In the case of 50 and 100 h grinders, a more homogeneous structure and smaller grained particles were observed in a manner similar to Fig. 4f and in accordance with the SEM results. Similar results are reported for Al-Si [44] and Cu-Al-Mn powder [45].

The thermal analysis used to define metastable structures is very important for technological applications [34, 46, 47]. So, thermal analyses are performed to determine the thermal behavior of the intermetallic phases of the alloyed $Al_{60}Cu_{20}Ni_{15}Ti_5$ powders. Thermal properties like phase transition temperatures of the alloyed powders are defined using the DTA, and the corresponding DTA thermograms are presented in Fig. 6. As shown in Fig. 6, the thermal behaviors of the alloys produced by grinding for 10–30 h are similar. They exhibit two obvious exothermic peaks indicating phase transition reactions. The first exothermic reaction of the 10–30 h milled powders appears at 350–400 ℃ temperature range. It can be attributed to the AlNi-phase formation. The second

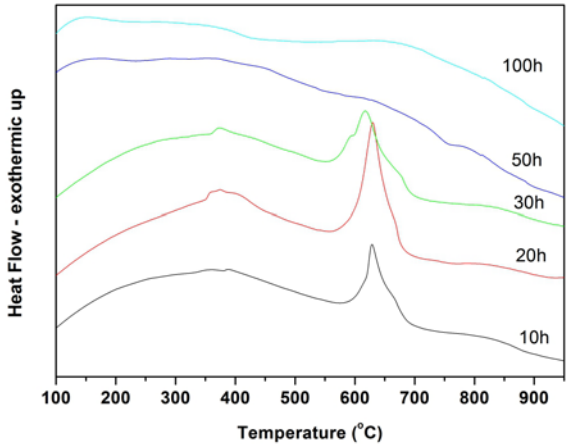


Fig. 6. DTA thermograms of mechanically milled $Al_{60}Cu_{20}Ni_{15}Ti_5$ powder as a function of milling time.

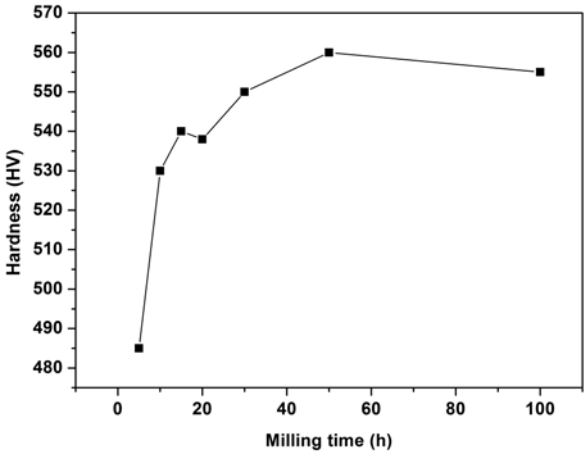


Fig. 7. Microhardness values of mechanically milled $Al_{60}Cu_{20}Ni_{15}Ti_5$ powders as a function of milling time after sintering at 700 ℃.

exothermic reaction indicating $Al_2Cu$-phase formation appears at 550–700 ℃ temperature range. These results were also seen in the XRD analysis for sintered samples. The broad peaks seen in the alloys produced by grinding at 50–100 h refer to the release of internal stress resulting from structural deformation and lattice strain. No peak expressing phase transformation was observed in these samples, because the NiTi-, $Al_3Ni$-, and AlNi-phases in the alloy are affected by more high temperatures. It is concluded that the novel complex $Al_{60}Cu_{20}Ni_{15}Ti_5$ alloy, which is a metastable formation, was produced by milling for 50 and 100 h.

Figure 7 shows the microhardness values obtained from the sintered $Al_{60}Cu_{20}Ni_{15}Ti_5$ alloy. As shown in Fig. 7, the average hardness of the samples increases in parallel with the milling time. This increase continues until the milling time of 50 h and reaches 560 HV, and the hardness values have decreased in the sample

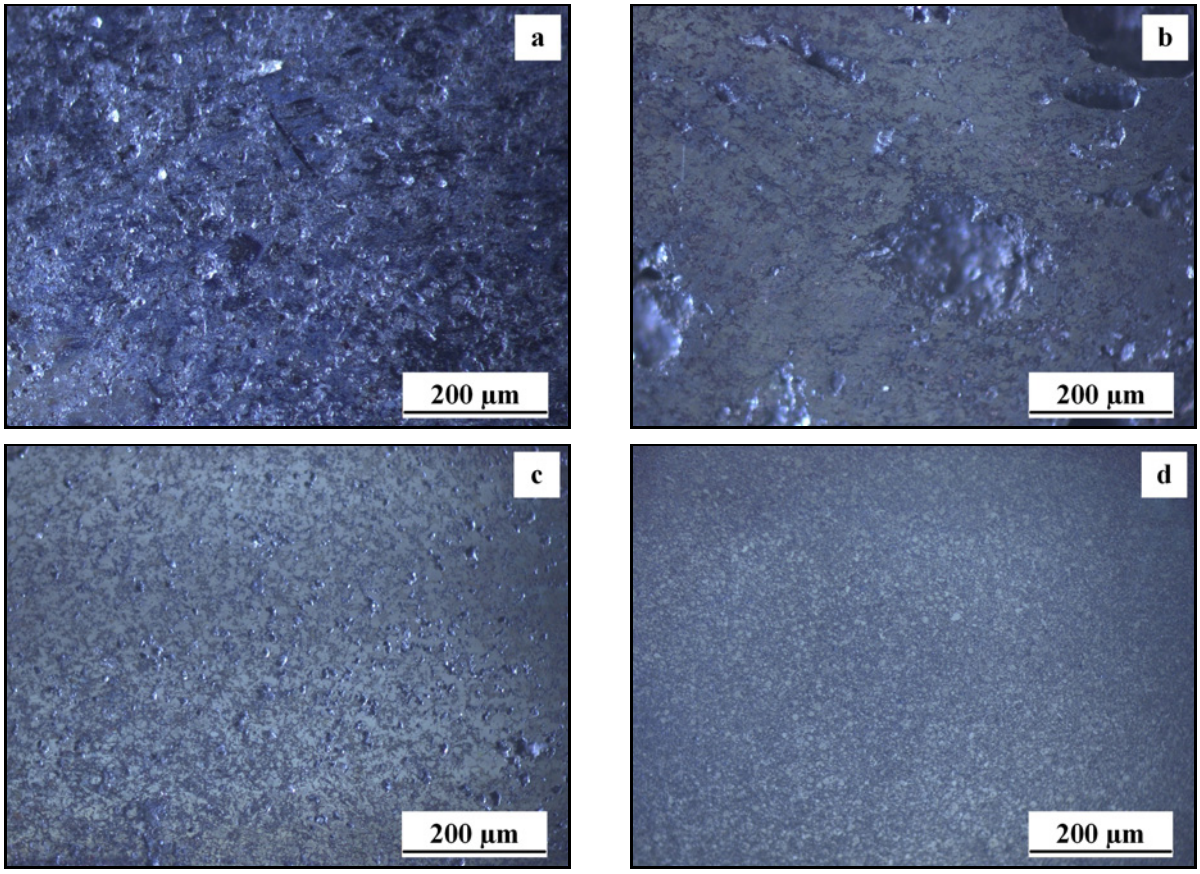


Fig. 8. POM images of mechanically milled $Al_{60}Cu_{20}Ni_{15}Ti_5$ powders as a function of milling time: (a) 5 h, (b)15 h, (c) 30 h, and (d) 100 h.

with a milling time of 100 h. After 100 h, it is possible to reduce the compressibility of the powder obtained and to affect the sintering process negatively. Since the samples produced with 100 h of grinding time cannot be appropriately pressed, the gaps between the particles increase, and dislocation is easier. This result is thought to have an impact on the decrease in the hardness values taken from the sintered sample. It is estimated that the reduction incompressibility of the powders obtained after 100 h of grinding is due to the increase in the viscosity of the powders and the fragile $Al_2Cu$-phase. It has been reported [48–51] that $Al_2Cu$-phase formation significantly reduces the hardness. Also, the surface images of the sintered samples taken by POM are shown in Fig. 8. As shown in Figs. 8a–d, as the milling time increases, the pore size and surface roughness of the material decrease.

## 4. Conclusions

In summary, the complex $Al_{60}Cu_{20}Ni_{15}Ti_5$ alloy was fabricated by mechanical alloying and sintering, and thermal and microstructural properties were investigated. The XRD results showed that intermetallic phases AlNi, NiTi, $Al_2Cu$, and $Al_3Ni$ in the novel complex $Al_{60}Cu_{20}Ni_{15}Ti_5$ alloy were formed; also, $Al_2O_3$--phase was observed due to the oxidation during sintering. The maximum microhardness value was found to be 560 HV as a result of the sintering of the alloy produced by grinding for 50 h. The DTA results showed that the AlNi-phase and $Al_2Cu$-phase formation occurred at a temperature range of 350–400 ℃ and 550–700 ℃, respectively, for 10–30 h milled powders and also indicated that the alloyed samples for 50–100 h were metastable formation. According to SEM/EDX results, a more homogeneous and spherical structure was observed as the milling time increased, and also, the crystallite size decreased. The crystallite size and the lattice strain of 100 h alloyed $Al_{60}Cu_{20}Ni_{15}Ti_5$ powders were found to be 10.5 nm and 0.87 %, respectively.

## Acknowledgement

We would like to thank the Batman University Scientific Research Projects Coordination for its financial support, Project No. 18.002.

## References


[1] Y. H. Kim, K. Hiraga, A. Inoue, T. Masumoto, H. H. Jo, Crystallization and high mechanical strength of Al-based amorphous alloys, Mater. Trans. JIM 35 (1994) 293–302. doi:10.2320/matertrans1989.35.293

[2] Y. H. Kim, A. Inoue, T. Masumoto, Ultrahigh tensile strengths of $Al_{88}Y_2Ni_9M_1$ (M = Mn or Fe) amorphous alloys containing finely dispersed fcc-Al particles, Mater. Trans. JIM 31 (1990) 747–749. doi:10.2320/matertrans1989.31.747

[3] I. T. H. Chang, R. R. Botten, Heat treatment of rapidly solidified Al-Ni-Mm alloys, Mater. Sci. Eng. A 226–228 (1997) 183–186. doi:10.1016/S0921-5093(97)80035-4

[4] W. T. Kim, M. Gogebakan, B. Cantor, Heat treatment of amorphous $Al_{85}Y_5Ni_{10}$ and $Al_{85}Y_{10}Ni_5$ alloys, Mater. Sci. Eng. A 226–228 (1997) 178–182. doi:10.1016/S0921-5093(96)10613-4

[5] D. Roy, R. Mitra, O. A. Ojo, S. S. Singh, D. Kolesnikov, W. Lojkowski, R. O. Scattergood, C. C. Koch, I. Manna, Evaluation of mechanical properties of partially amorphous and nanocrystalline $Al_{50}Ti_{40}Si_{10}$ composites prepared by mechanical alloying and hot isostatic pressing, Mater. Sci. Eng. A 555 (2012) 21–27. doi:10.1016/j.msea.2012.06.028

[6] V. V. Dabhade, T. R. Rama Mohan, P. Ramakrishnan, Nanocrystalline titanium powders by high energy attrition milling, Powder Technol. 171 (2007) 177–183. doi:10.1016/j.powtec.2006.10.007

[7] M. J. Phasha, A. S. Bolokang, P. E. Ngoepe, Solid-state transformation in nanocrystalline Ti induced by ball milling, Mater. Lett. 64 (2010) 1215–1218. doi:10.1016/j.matlet.2010.02.054

[8] B. Avar, S. Ozcan, Structural evolutions in Ti and $TiO_2$ powders by ball milling and subsequent heat-treatments, Ceram. Int. 40 (2014) 11123–11130. doi:10.1016/j.ceramint.2014.03.137

[9] T. Masumoto, Recent progress in amorphous metallic materials in Japan, Mater. Sci. Eng. A 179/180 (1994) 8–16. doi:10.1016/0921-5093(94)90155-4

[10] C. S. Kiminami, N. D. Basim, M. J. Kaufman, M. F. Amateau, T. J. Eden, G. J. Galbraith, Challenges in the development of aluminium-based bulk amorphous alloys, Key Eng. Mater. 189–191 (2001) 503–508. doi:10.4028/www.scientific.net/KEM.189-191.503

[11] A. Inoue, Stabilization of metallic supercooled liquid and bulk amorphous alloys, Acta Mater. 48 (2000) 279–306. doi:10.1016/S1359-6454(99)00300-6

[12] J. Eckert, L. Schultz, K. Urban, Formation of quasicrystals by mechanical alloying, Appl. Phys. Lett. 55 (1989) 117–119. doi:10.1063/1.102394

[13] M. S. El-Eskandarany, K. Aoki, K. Suzuki, Mechanically induced cyclic crystalline amorphous transformations of ball milled $Co_{50}Ti_{50}$ alloy, Scripta Mater. 36 (1997) 1001–1009. doi:10.1016/S1359-6462(97)00011-0

[14] M. Gazizov, C. D. Marioara, J. Friis, S. Wenner, R. Holmestad, R. Kaibyshev, Precipitation behavior in an Al-Cu-Mg-Si alloy during aging, Mater. Sci. Eng. A 767 (2019) 138369. doi:10.1016/j.msea.2019.138369

[15] H. G. Tang, Z. Q. Cheng, J. W. Liu, X. F. Ma, Preparation of a high strength Al-Cu-Mg alloy by mechanical alloying and press-forming, Mater. Sci. Eng. A 550 (2012) 51–54. doi:10.1016/j.msea.2012.04.016

[16] Z. Fu, W. Chen, Z. Chen, H. Wen, E. J. Lavernia, Influence of Ti addition and sintering method on microstructure and mechanical behavior of a medium-entropy $Al_{0.6}CoNiFe$ alloy, Mater. Sci. Eng. A 619 (2014) 137–145. doi:10.1016/j.msea.2014.09.077

[17] A. Munitz, M. J. Kaufman, J. P. Chandler, H. Kalaantari, R. Abbaschian, Melt separation phenomena in CoNiCuAlCr high entropy alloy containing silver, Mater. Sci. Eng. A 560 (2013) 633–642. doi:10.1016/j.msea.2012.10.007

[18] A. Cunliffe, J. Plummer, I. Figueroa, I. Todd, Glass formation in a high entropy alloy system by design, Intermetallics 23 (2012) 204–207. doi:10.1016/j.intermet.2011.12.006

[19] T. M. Yue, H. Xie, H. O. Yang, G. H. Meng, Solidification behaviour in laser cladding of AlCoCrCuFeNi high-entropy alloy on magnesium substrates, J. Alloy. Compd. 587 (2014) 588–593. doi:10.1016/j.jallcom.2013.10.254

[20] A. Takeuchi, N. Chen, T. Wada, Y. Yokoyama, H. Kato, A. Inoue, J. W. Yeh, $Pd_{20}Pt_{20}Cu_{20}Ni_{20}P_{20}$ high-entropy alloy as a bulk metallic glass in the centimeter, Intermetallics 19 (2011) 1546–1554. doi:10.1016/j.intermet.2011.05.030

[21] M. Gogebakan, C. Kursun, J. Eckert, Formation of new Cu-based nanocrystalline powders by mechanical alloying technique, Powder Technol. 247 (2013) 172–177. doi:10.1016/j.powtec.2013.07.019

[22] D. K. Misra, R. S. Tiwari, O. N. Srivastava, Devitrification of rapidly quenched Al-Cu-Ti amorphous alloys, Bull. Mater. Sci. 26 (2003) 553–558. doi:10.1007/BF02707356

[23] M. Gogebakan, B. Avar, M. Tarakci, Microstructures and mechanical properties of conventionally solidified $Al_{63}Cu_{25}Fe_{12}$ alloy, J. Alloy. Compd. 509S (2011) S316–S319. doi:10.1016/j.jallcom.2010.10.179

[24] B. Avar, M. Gogebakan, F. Yilmaz, Characterization of the icosahedral quasicrystalline phase in rapidly solidified Al-Cu-Fe alloys, Zeitschrift für Kristallographie 223 (2008) 731–734. doi:10.1524/zkri.2008.1077

[25] I. Boromei, A. Casagrande, F. Tarterini, G. Poli, P. Veronesi, R. Rosa, Ni-Al-Ti coatings obtained by microwave assisted SHS: Oxidation behaviour in the 750–900 °C range, Surf. Coat. Technol. 204 (2010) 1793–1799. doi:10.1016/j.surfcoat.2009.11.018

[26] S. Varalakshmi, G. A. Rao, M. Kamaraj, B. S. Murty, Hot consolidation and mechanical properties of nanocrystalline equiatomic AlFeTiCrZnCu high entropy alloy after mechanical alloying, J. Mater. Sci. 45 (2010) 5158–5163. doi:10.1007/s10853-010-4246-5

[27] Z. Chen, W. Chen, B. Wu, X. Cao, L. Liu, Z. Fu, Effects of Co and Ti on microstructure and mechanical behavior of $Al_{0.75}FeNiCrCo$ high entropy alloy prepared by mechanical alloying and spark plasma sintering, Mater. Sci. Eng. A 648 (2015) 217–224. doi:10.1016/j.msea.2015.08.056

[28] J. M. Wu, S. J. Lin, J. W. Yeh, S. K. Chen, Y. S. Huang, H. C. Chen, Adhesive wear behavior of $Al_xCoCrCuFeNi$ high-entropy alloys as a function of aluminum content, Wear 261 (2006) 513–519. doi:10.1016/j.wear.2005.12.008

[29] C. J. Tong, M. R. Chen, S. K. Chen, J. W. Yeh, T. T. Shun, S. J. Lin, S. Y. Chang, Mechanical performance of the $Al_xCoCrCuFeNi$ high-entropy alloy system with

multiprincipal elements, Metall. Mater. Trans. A 36 (2005) 1263–1271. doi:10.1007/s11661-005-0218-9
[30] C. Z. Yao, P. Zhang, M. Liu, G. R. Li, J. Q. Ye, P. Liu, Y. X. Tong, Electrochemical preparation and magnetic study of Bi-Fe-Co-Ni-Mn high entropy alloy, Electrochim. Acta 53 (2008) 8359–8365. doi:10.1016/j.electacta.2008.06.036
[31] D. Roy, S. S. Singh, R. Mitra, M. Rosinski, A. Michalski, W. Lojkowski, I. Mannaet, Synthesis and characterization of precipitation hardened amorphous matrix composite by mechanical alloying and pulse plasma sintering of $Al_{65}Cu_{20}Ti_{15}$, Philosophical Magazine 89 (2009) 1051–1061. doi:10.1080/14786430902859784
[32] Z. Tan, Y. F. Xue, L. Wang, X. W. Cheng, L. Zhang, H. F. Zhang, A. M. Wanget, Alloying evolution and stability of $Al_{65}Cu_{20}Ti_{15}$ during process of amorphisation by high energy ball milling, Powder Metall. 55 (2012) 361–367. doi:10.1179/1743290112Y.0000000005
[33] C. Suryanarayana, Mechanical alloying and milling, Progress in Materials Science 46 (2001) 1–184. doi:10.1016/S0079-6425(99)00010-9
[34] C. Kursun, M. Gogebakan, Characterization of nanostructured Mg-Cu-Ni powders prepared by mechanical alloying, J. Alloy. Compd. 619 (2015) 138–144. doi:10.1016/j.jallcom.2014.08.126
[35] D. H. Kim, W. T. Kim, D. H. Kim, Formation and crystallization of Al-Ni-Ti amorphous alloys, Mater. Sci. Eng. A 385 (2004) 44–53. doi:10.1016/j.msea.2004.04.016
[36] H. H. Sheu, L. C. Hsiung, J. R. Sheu, Synthesis of multiphase intermetallic compounds by mechanical alloying in Ni-Al-Ti system, J. Alloy. Compd. 469 (2009) 483–487. doi:10.1016/j.jallcom.2008.02.019
[37] A. Samanta, H. J. Fecht, I. Manna, P. P. Chattopadhyay, Development of amorphous phase dispersed Al-rich composites by rolling of mechanically alloyed amorphous Al-Ni-Ti powders with pure Al, Mater. Chem. Phys. 104 (2007) 434–438. doi:10.1016/j.matchemphys.2007.03.041
[38] H. M. Lin, C. Y. Chen, C. Y. Tsay, C. F. Hsu, P. Y. Lee, Microstructure and mechanical properties of mechanically alloyed $Al_2O_3$/Ti-Cu-Ni-Sn bulk metallic glass composites prepared by vacuum hot-pressing, J. Alloy Compd. 504S (2010) S110–S113. doi:10.1016/j.jallcom.2010.02.026
[39] C. Suryanarayana, M. G. Norton, X-ray Diffraction: A Practical Approach. Plenum Press, New York, 1998. ISBN: 978-1-4899-0148-4.
[40] J. I. Langford, A. J. C. Wilson, Scherrer after sixty years: A survey and some new results in the determination of crystallite size, J. Appl. Cryst. 11 (1978) 102–113. doi:10.1107/S0021889878012844
[41] N. S. Gonçalves, J. A. Carvalho, Z. M. Lima, J. M. Sasaki, Size–strain study of NiO nanoparticles by X-ray powder diffraction line broadening, Mater. Lett. 72 (2012) 36–38. doi:10.1016/j.matlet.2011.12.046
[42] B. D. Cullity, S. R. Stock, Elements of X-ray Diffraction, 3rd Edition, Prentice-Hall, Upper Saddle River, New Jersey, 2001. ISBN-10: 0201610914, ISBN-13: 978-0201610918.
[43] B. AlMangour, D. Grzesiak, J. M. Yang, In situ formation of TiC-particle-reinforced stainless steel matrix nanocomposites during ball milling: Feedstock powder preparation for selective laser melting at various energy densities, Powder Technol. 326 (2018) 467–478. doi:10.1016/j.powtec.2017.11.064
[44] W. K. Kang, F. Yilmaz, H. S. Kim, J. M. Koo, S. J. Hong, Fabrication of Al-20wt.%Si powder using scrap Si by ultra high-energy milling process, J. Alloy Compd. 536 (2012) 45–49. doi:10.1016/j.jallcom.2012.01.106
[45] M. R. Rezvani, A. Shokuhfar, Synthesis and characterization of nanostructured Cu-Al-Mn shape memory alloy by mechanical alloying, Mater. Sci. Eng. A 532 (2012) 282–286. doi:10.1016/j.msea.2011.10.093
[46] J. J. Suñol, J. M. Güell, J. Bonastre, S. Alleg, Structural study of nanocrystalline Fe-Co-Nb-B alloys prepared by mechanical alloying, J. Alloy. Compd. 483 (2009) 604–607. doi:10.1016/j.jallcom.2008.07.212
[47] L. Shaw, H. Luo, J. Villegas, D. Miracle, Thermal stability of nanostructured $Al_{93}Fe_3Cr_2Ti_2$ alloys prepared via mechanical alloying, Acta Mater. 51 (2003) 2647–2663. doi:10.1016/S1359-6454(03)00075-2
[48] P. P. Ma, C. H. Liu, C. L. Wu, L. M. Liu, J. H. Chen, Mechanical properties enhanced by deformation-modified precipitation of q-phase approximants in an Al-Cu alloy, Mater. Sci. Eng. A 676 (2016) 138–145. doi:10.1016/j.msea.2016.08.068
[49] A. Mostaed, H. Saghafian, E. Mostaed, A. Shokuhfar, H. R. Rezaie, Effect of reinforcing particle type on morphology and age-hardening behavior of Al-4.5wt.%Cu based nanocomposites synthesized through mechanical milling, Mater. Charact. 76 (2013) 76–82. doi:10.1016/j.matchar.2012.12.007
[50] S. Arakawa, T. Hatayama, K. Matsugi, O. Yanagisawa, Effect of heterogeneous precipitation on age hardening of $Al_2O_3$ particle dispersion Al-4mass%Cu composite produced by mechanical alloying, Scripta Mater. 42 (2000) 755–760. doi:10.1016/S1359-6462(99)00426-1
[51] M. A. Taha, G. M. Elkomy, H. A. Mostafa, E. S. Gouda, Effect of $ZrO_2$ contents and ageing times on mechanical and electrical properties of Al-4.5wt.%Cu nanocomposites prepared by mechanical alloying, Mater. Chem. Phys. 206 (2018) 116–123. doi:10.1016/j.matchemphys.2017.11.058